LBL-14802
Preprint c.2

Lawrence Berkeley Laboratory

UNIVERSITY OF CALIFORNIA

RECEIVED
LAWRENCE
BERKELEY LABORATORY

SEP 30 1982

LIBRARY AND
DOCUMENTS SECTION

Materials & Molecular Research Division

Submitted to Journal of Magnetic Resonance

ELECTRICALLY DETECTED ELECTRON PARAMAGNETIC RESONANCE IN GERMANIUM SINGLE CRYSTALS

E.J. Pakulis

August 1982

TWO-WEEK LOAN COPY

This is a Library Circulating Copy which may be borrowed for two weeks. For a personal retention copy, call Tech. Info. Division, Ext. 6782.

LBL-14802 c.2

DISCLAIMER

This document was prepared as an account of work sponsored by the United States Government. While this document is believed to contain correct information, neither the United States Government nor any agency thereof, nor the Regents of the University of California, nor any of their employees, makes any warranty, express or implied, or assumes any legal responsibility for the accuracy, completeness, or usefulness of any information, apparatus, product, or process disclosed, or represents that its use would not infringe privately owned rights. Reference herein to any specific commercial product, process, or service by its trade name, trademark, manufacturer, or otherwise, does not necessarily constitute or imply its endorsement, recommendation, or favoring by the United States Government or any agency thereof, or the Regents of the University of California. The views and opinions of authors expressed herein do not necessarily state or reflect those of the United States Government or any agency thereof or the Regents of the University of California.

ELECTRICALLY DETECTED ELECTRON PARAMAGNETIC RESONANCE IN GERMANIUM SINGLE CRYSTALS*

E. J. Pakulis

Materials and Molecular Research Division,
Lawrence Berkeley Laboratory, and
Department of Physics,
University of California, Berkeley, CA 94720

August 1982

*This work was supported by the Director, Office of Energy Research, Office of Basic Energy Sciences, Materials Science Division of the U.S. Department of Energy under Contract Number DE-AC03-76SF00098.

ABSTRACT

The results of ultra-high sensitivity EPR studies of Ge single crystals are discussed. Maximum sensitivity was achieved by using high Q microwave resonant samples together with an electric detection technique. Under sub band-gap optical excitation, two sets of lines were detected: four lines with axial symmetry about the four ⟨111⟩ axes with $g_{\parallel} = 0.34$ and $g_{\perp} = 1.94$, and 24 lines with $g_{\parallel} = 0.73$ and $g_{\perp} = 1.89$, axially symmetric about ⟨111⟩ axes with a six-fold 1.2° distortion. Detection involved monitoring the absorption of energy from the microwave electric field by photo-excited electrons. Due to spin dependent scattering of the electrons by dangling bonds located in the core of dislocations within the crystal, a resonant change in this absorption was observed on each passage through spin resonance. Both increases and decreases in the absorption were observed, depending on sample characteristics. The spin dependent scattering was observed to persist for hours after the removal of optical excitation, indicating the existence of a conducting dislocation band with a very long lifetime.

Electron paramagnetic resonance (EPR) (*1*) has been used widely, and with a great deal of success, in the study of defects in semiconductors. Valuable information can be obtained not only about the identity of a defect, but sometimes also about its microscopic structure. Corbett et al. (*2*) give a good review of the extent to which this powerful technique has been utilized in studies of a long list of semiconductors. Of the elemental semiconductors, silicon has been most extensively studied, while germanium, by comparison, has had strikingly few reports of EPR spectra. The primary reason for this is the inhomogeneous broadening of lines in germanium which leads to a reduction in signal amplitude. The broadening results from unresolved hyperfine structure of the Ge^{73} nucleus, with a spin I = 9/2 and an isotopic abundance of 7.76%, and, even more importantly, from nonuniform strains in the crystal. The strain broadening is a direct result of the large spin-orbit interaction in Ge (*3*). The present work shows that these difficulties are not insurmountable and that we can expect to see the continued successful application of EPR to the study of defects in germanium.

A number of interesting features have surfaced during the course of this work. First, there was the observation of spin-dependent photoconductivity in the germanium samples containing dislocations. Spin-dependent photoconductivity arises when the number and/or the mobility of photo-excited free carriers depends on their spin orientation relative to that of their recombination and/or scattering centers. Then, there was the discovery that the spin-dependent conductivity remains long after the removal of optical excitation. This observation led to the conclusion that free carriers can relax into a long lifetime dislocation band,

retaining a non-zero, spin-dependent mobility. Next, the spin-dependent conductivity along dislocations made possible the measurement of the g-tensor of the dislocation dangling bond electrons using the method of electric detection of magnetic resonance. In this method the mobile charges are accelerated by a microwave electric field, their absorption of energy being directly related to their spin polarization (relative to that of their scattering centers, i.e. dangling bond electrons) through their spin-dependent conductivity. Perhaps the most significant result of this study was the determination of a small, very well-defined distortion angle of the dislocation dangling bonds. This determination was made directly from the symmetry, multiplicity, and splitting of the lines in the EPR spectrum. There is the intriguing possibility that the distortion of the dangling bonds may be the result of a Peierls transition along the dislocation line.

Before going any further, it will be helpful to briefly discuss dislocations in the tetrahedral crystal structure. Dislocation lines are characterized by a Burgers vector giving the magnitude and direction of the displacement of one part of the crystal relative to the rest of the crystal. The part of the Burgers vector parallel to the dislocation is the screw component, that part perpendicular to the dislocation is the edge component. The two extreme cases - 100% screw and 100% edge - are illustrated in Figure 1. In the diamond structure, dislocation lines run along ⟨110⟩ directions and often have Burgers vectors at 60° (*4*). These are the so-called 60°-dislocations and have been studied extensively (*5*). They can occur in at least two basic varieties, the shuffle set and the glide set, depending on which set of bonds were broken in the creation

of the dislocation. If the bonds broken were perpendicular to the dislocation line, one ends up with the shuffle set; otherwise, one has the glide set. This simple picture is helpful conceptually, but in real crystals one encounters many complications, the details of which are not entirely understood. For example, one can have kinks in dislocation lines, or lines of the shuffle set can become associated with stacking faults, or lines of the glide set can dissociate into partial dislocations - so long as the sum of the Burgers vectors of the partials equals the Burgers vector of the original line. For the purposes of discussion, the model adopted here is that of the 60°-dislocation of the shuffle set, pictured in Figure 2. The figure shows the Burgers vector, $\vec{b}$, and the dislocation line, d, with its row of broken bonds. These are the so-called dislocation dangling bonds, which to first order can be thought of as sp^3 orbitals, each containing one electron with spin 1/2.

It has been expected for three decades that the dislocation dangling bond electrons should be observable using magnetic resonance techniques. It was not until 1964 that Alexander, Labusch, and Sander (7) first observed electron spin resonance at dislocation dangling bonds in silicon. The silicon had been plastically deformed to increase the number of dislocations to a density of $\sim 10^8$ cm^{-2}. Why wasn't something similar seen in germanium? One possibility is that plastic deformation of germanium, although resulting in high densities of dislocations, may not increase the amplitude of the signal enough to make it observable, due to increased strain broadening. Throughout this work, only as-grown crystals were studied, with dislocation densities $\sim 10^4$ cm^{-2}.

Without the aid of large numbers of artificially induced dislocations, one needs several orders of magnitude greater sensitivity to detect the spin resonance of the dislocation dangling bond electrons. This greater sensitivity was achieved through the use of high-Q microwave resonant samples and electric detection of magnetic resonance.

Electric Detection of Magnetic Resonance.

Electric detection of magnetic resonance is most easily introduced by analogy to the widely used technique of optical detection of magnetic resonance (*8*). In the latter, one observes the spin resonance of two species giving rise to recombination luminescence by monitoring some aspect of the luminescence (i.e. intensity or polarization) which depends on the spin polarization of the species. In electric detection, instead of looking at spin-dependent luminescence, one looks at spin-dependent conductivity.

The sample is placed in the microwave cavity of an EPR spectrometer. Optical pumping is used, if necessary, to excite conduction electrons. If the conductivity changes during spin resonance, so does the absorption of energy, by the free carriers, from the microwave electric field. It is this change in absorption which is detected as a change in cavity Q, and in general it can be of either sign. If the conductivity increases, the absorption increases and the Q decreases as for an ordinary absorptive signal. If the conductivity decreases, the absorption decreases and the Q increases as for an emissive signal.

Dependence of the conductivity on spin polarization can result from spin dependent scattering processes and/or spin dependent recombination

processes. Numerous examples of this effect can be found in the literature. Honig considered the neutral impurity scattering of highly spin-polarized carriers in semiconductors (*9*). He suggested that Zeeman spectroscopy of the neutral shallow donors could be carried out by observing changes in photo-conductivity occurring during changes in spin polarization. Maxwell and Honig did the experiment for the case of the phosphorous donor in silicon.

The basic idea involved is that the triplet scattering cross-section (carrier and scatterer have parallel spins) differs from the singlet scattering cross-section (carrier and scatterer have anti-parallel spins), and the percentage of triplet scattering events is a function of the spin polarization. The net result is that the conductivity is spin dependent because the mobility of carriers is a function of spin polarization.

For a more quantitative description, consider the following simple model. Let

$n = n\uparrow + n\downarrow$ = concentration of mobile electrons with spin 1/2

$N = N\uparrow + N\downarrow$ = concentration of scattering centers with spin 1/2

$p = (n\uparrow - n\downarrow)/n$ = spin polarization of mobile electrons

$P = (N\uparrow - N\downarrow)/N$ = spin polarization of scattering centers

X_s = singlet scattering cross section

X_t = triplet scattering cross section

The probability of singlet scattering is given by $(1-pP)/4$, and the probability of triplet scattering by $(3+pP)/4$, so that the total scattering cross section is just

$$X = X_s(1-pP)/4+X_t(3+pP)/4. \qquad [1]$$

The conductivity is proportional to 1/X. If either one of the spin transitions is saturated, i.e. p = 0 or P = 0, the change in X is $pP(X_s-X_t)/4$ and the fractional change in conductivity is

$$\Delta\sigma/\sigma = pP(X_t - X_s)/(X_s + 3X_t). \qquad [2]$$

The important points to note are that the absolute value of the change in conductivity increases with increasing polarization and increasing spin dependence of the scattering cross section, and that $\Delta\sigma$ can be of either sign, depending on the sign of (X_t-X_s).

Lepine and Prejean (*10*) reported spin-dependent photoconductivity in silicon in which the number of carriers was a function of the spin polarization of their recombination centers. Instead of triplet and singlet scattering cross-sections, one has triplet and singlet capture cross-sections, and thus a recombination rate depending on spin polarization. The recombination centers responsible were thought to be paramagnetic surface centers. Kurylev and Karyagin (*11*, *12*) observed spin-dependent recombination at surface sites in germanium.

Spin-dependent photoconductivity in plastically deformed silicon was investigated by two groups independently. Grazhulis et al. (*13*) observed, in p-type deformed silicon at liquid helium temperatures, a resonant decrease in photoconductivity coincident with the spin resonance of the dislocation spin system. They attributed their results to the spin dependence of the scattering of free carriers by dislocations. Wosinski and Figielski (*14*) made a similar observation in n-type deformed silicon at temperatures between 80 and 340 K, but attributed their results to spin dependent recombination of free electrons at dislocations. Wosinski et al. (*15*) describe a contactless method for measuring the spin dependent

photoconductivity in which they monitor the change in Q of a cavity loaded with the sample. Their contactless method is exactly equivalent to electric detection of magnetic resonance. Since conventional EPR results were already available for the silicon dislocation spin system, both groups were able to make a direct comparison between their spin-dependent photoconductivity spectrum and the EPR spectrum. Spin-dependent increases in conductivity were observed by Szkielko (*16*) in dislocated silicon p-n junctions. He attributed his results to spin-dependent generation of carriers at dislocations.

The results of the spin-dependent photoconductivity studies of dislocated silicon were of considerable aid in the interpretation of the results to be presented here.

Experimental Details.

All experiments were conducted on a 1 cm superheterodyne spectrometer, a block diagram of which appears in Figure 3. Magnetic field modulation and lock-in detection were used to record the derivative of the absorption signal.

Figure 4 is a blowup of the end of the waveguide together with a cross-section of the tunable cylindrical cavity. Optical pumping was possible through a window at the bottom of the dewar and a hole in the bottom of the cavity. A PEK 203 mercury vapor arc lamp was used with some combination of the filters listed in Table 1. With no filters, 0.1 watts reached the sample. An aluminum shutter was mounted directly beneath the cavity in the helium bath and could be rotated from outside the dewar via a stainless steel rod. This allowed the measurement of the dark

spectrum and of the decay of the light-induced spectrum. The cavity was centered between the pole pieces of the magnet, which could be rotated in the horizontal plane. The field was measured with a rotating coil gaussmeter, and had an upper limit of 19 kgauss. Calibration was achieved using a g-marker of powdered phosphorous doped silicon embedded in polyethylene, provided by E. A. Gere. All experiments were performed with the sample immersed in liquid helium, usually at temperatures 1.8-1.9 K, achieved by mechanically pumping the helium vapor.

Samples were cut from Czochralski-grown single crystals of lightly doped n-type germanium supplied by W. L. Hansen and E. E. Haller of Lawrence Berkeley Laboratory. Most of the samples were cut in the shape of right circular cylinders using an ultrasonic cutter. They had diameters of 12.5 mm and heights ranging from 8 to 10 mm. The axis of the cylinder was chosen to be either a ⟨100⟩ or a ⟨110⟩ crystal axis. A few of the samples were rectangular parallelopipeds. Results were insensitive to surface preparation.

Table 2 summarizes sample characteristics. Net donor concentrations were in the range 5×10^9 to 8×10^{13} cm^{-3}. With the exception of one dislocation-free sample, dislocation etch pit densities were between 10^3 and 10^5 cm^{-2}, but were not uniform and should only be regarded as order of magnitude estimates. Diverse crystal growing conditions were selected to study which factors did or did not influence the results. All S-crystals (see Table 2) were grown in one crystal-growing apparatus, the rest of the crystals in another. The growth axes of the crystals were either ⟨100⟩ or ⟨111⟩, the growth atmospheres were hydrogen, deuterium, argon, or vacuum, and the crucible materials were either quartz or graphite.

The typical sample was lapped, chemically etched, and mounted with styrofoam in the spectrometer cavity. When cooled to liquid helium temperatures, the sample itself becomes a microwave resonant dielectric cavity with a large quality factor $Q \approx 10^5$ (*17*). This high Q was essential in achieving the required sensitivity.

Two different experimental geometries were used. Most often the magnetic field was rotated in a plane nearly parallel to a (110) plane of the crystal, which is the only plane containing all three principal directions - ⟨100⟩, ⟨110⟩, and ⟨111⟩. In the second geometry, the field was rotated in a (100) plane. The angle between the magnetic field and the tetrahedral axes was determined by observing the angular dependence of the electron cyclotron resonances in the sample.

Results.

Two new sets of EPR lines (*18*) were observed in optically excited n-type germanium samples containing dislocations: 24 narrow lines (14 gauss peak-to-peak derivative width), and four broad lines (20 to 60 gauss peak-to-peak). Both spectra are associated with electrons at dislocations. The lines persist for hours after excitation and can be of either sign, i.e. absorptive or emissive. When the magnetic field is along a ⟨100⟩ axis, all 28 lines converge to the simple spectrum centered at g = 1.6 shown in Figure 5, adjacent to the arsenic donor hyperfine structure.

As the magnetic field was rotated away from the ⟨100⟩ axis, the lines proved to be highly anisotropic. Figure 6 is a plot of the angular dependence of the 24 narrow lines when the magnetic field was rotated approximately in the (110) plane. The spectrum consists of four main

branches - two with six resolved lines each, and two branches which appear to have only three lines but actually become resolved into six when the magnetic field is rotated in a different plane. The overall symmetry of the four branches is that of the four ⟨111⟩ axes, so each ⟨111⟩ axis contributes six narrow lines. The two branches with six resolved lines each would have become superposed had the magnetic field been exactly in the (110) plane. The line intensities from each of the four ⟨111⟩ axes are in general not equal, the relative intensities being sample dependent.

When the magnetic field was rotated in the approximate (100) plane, the spectrum in Figure 7 was observed. Again, due to the slight misorientation, the contributions from the four ⟨111⟩ axes can be readily identified. Because the lower branch in the insert had an order of magnitude smaller signal than the upper branch, only four of the six lines were seen.

Misalignment was an aid in untangling the narrow lines, but near perfect alignment was needed to be able to track the broad lines over a large range of g values. The spectrum of the broad lines is shown in Figure 8. There is one line per ⟨111⟩ axis, but for perfect orientation in a (100) plane there are two pair of equivalent ⟨111⟩ axes.

All the data can be described by an effective spin Hamiltonian containing only the electronic Zeeman interaction term:

$$\mathcal{H} = \beta \vec{H} \cdot \overleftrightarrow{g} \cdot \vec{S} \ . \qquad [3]$$

Here β is the Bohr magneton, $\vec{H}$ the magnetic field, $\overleftrightarrow{g}$ the spectroscopic splitting tensor, and $\vec{S}$ the effective spin. The four broad lines arise from a spin 1/2 species with g axially symmetric about the four ⟨111⟩ axes with

$$g_{\parallel} = 0.34 \text{ and } g_{\perp} = 1.94 \ . \qquad [4]$$

The 24-line spectrum is identical to one resulting from spin 1/2 sites with the 24 symmetry axes,

$$\langle 111 \rangle_i \pm \alpha \langle 110 \rangle_k \ , \qquad [5]$$

where i = 1 to 4 and k = 1 to 6, subject to the condition $\langle 111 \rangle \cdot \langle 110 \rangle = 0$, with $\alpha = 0.021$. The significance of α will be discussed later. The principal g values for the narrow lines are

$$g_{\parallel} = 0.73 \text{ and } g_{\perp} = 1.89 \ . \qquad [6]$$

A comparison with g values for other defects in Ge appears in Table 3.

Neither the four-line spectrum nor the 24-line spectrum was seen prior to illumination of the sample. Radiation from the 300 K window was sufficient to induce both spectra, but the effectiveness of this mode of excitation was sample dependent. Between 10 and 1000% enhancement could be achieved by optical pumping with a mercury vapor arc lamp through a 2 mm thick room temperature Ge filter, the size of the enhancement being sample dependent. Typically, samples in which the window radiation was least effective underwent the largest enhancements. The intensity of the light had a pronounced effect on the shape of the lines. Figure 9 shows the effect of placing a 10 db neutral density filter in front of the lamp. The lines were absent during illumination with the totally unfiltered arc lamp, but were maximized after such illumination. Presumably, the holes created while pumping above the band gap combine with dangling bonds to cause extinction of the signal. The set of long pass filters listed in Table 1 was used to determine the photon energies required for signal enhancement. Each long pass filter was used in conjunction with the Ge

filter and the 20 db neutral density filter. The size of the arsenic hyperfine structure was monitored to check for any changes in coupling of the mode to the cavity. The results are shown in Figure 10. Enhancement sets in at a photon energy of about 600 meV.

Varying the microwave power into the cavity had a pronounced effect on the shape of the lines. Figure 11 shows one of the broad lines at (a) 0.5×10^{-8} watts and at (b) 0.5×10^{-6} watts. At low power the ambiguity as to the sign of the line is eliminated. Figure 12 compares several of the narrow lines at (a) 0.5×10^{-8} watts and at (b) 0.5×10^{-7} watts. All samples showed qualitatively the same behavior, but due to variations from sample to sample a quantitative study was not attempted.

Since optical excitation was required to induce the lines, it was of interest to study the decay of the spectrum after the removal of the excitation source. In general, the signal amplitude decreased during the first 20 minutes after closing the shutter and then levelled off. The amplitude was monitored for up to three hours 50 minutes, and once it had levelled off it showed no signs of further decay. The percentage drop in the first 20 minutes was sample dependent but typically fell into the range 60 to 80%. Time dependences for two samples at opposite ends of this range are plotted in Figure 13. The absence of any electron cyclotron resonance signal confirmed that there were no light leaks. EPR of an equally long-lived photo-induced excited state has been reported for dislocated Si (*22*).

Relation to Dislocations.

How does one know that these two new spectra arise from electrons at dislocations? The first piece of evidence is the failure to observe the spectra in a dislocation-free sample. All the other characteristics (see Table 2) of that sample were the same as for crystals which did give the new lines; in particular, normal shallow donor hyperfine structure and cyclotron resonance signals were observed.

Further evidence that the new spectra are related to dislocations is the large discrepancy between the line intensities from each of the ⟨111⟩ axes. This behavior is explicable for a distribution of spins on line defects, but not point defects. If the spins were distributed on isolated point defects, the ⟨111⟩ directions, being equivalent, would each have a probability 1/4 of being occupied, and one would see very nearly equal contributions from the four axes. In the case of dislocations, however, once they begin to nucleate in the plane perpendicular to a given axis, it would require energy to turn out of that plane. The result is a preponderance of dislocations in one plane. The line intensity from one of the ⟨111⟩ axes was typically five to ten times that of the others. The extreme case was the vacuum-grown crystal, in which a signal was observed exclusively from one axis. Another interesting case was the ⟨111⟩ grown crystal in which no signal was observed from the growth axis, i.e., there were no dislocations perpendicular to the growth axis.

Additional evidence linking the new spectra to dislocations is the symmetry of the 24-line spectrum. Expression [5] for the symmetry axes specifically relates each ⟨111⟩ axis to the three ⟨110⟩ axes perpendicular to it. As already mentioned, dislocation lines in the tetrahedral

structure run along ⟨110⟩ directions, so the results are consistent with a model in which the signal is due to dislocation dangling bonds which are nearly perpendicular to the dislocation lines.

Yet another connection to dislocations is seen in the sign reversal of the lines in crystals grown in hydrogen and/or deuterium atmospheres. For the usual EPR magnetic dipole absorption lines, as detected by the magnetic field of the cavity, sign reversal could result from an inverted spin population created by spin dependent relaxation processes present in the optical pumping cycle. This interpretation, however, cannot explain the persistence of the lines for hours after removal of optical excitation and after repeated passage through spin resonance. The signal reversal *can* be understood within the framework of spin dependent conductivity and electric detection of magnetic resonance. Figure 14 is a blowup of a dislocation line, showing schematically triplet and singlet scattering of two photo excited electrons by dangling bond electrons. Recall that the relative magnitude of the singlet and triplet scattering cross-sections determines the sign of the lines. According to this model, crystals grown in hydrogen and/or deuterium have a larger singlet scattering cross-section, while the opposite is true for vacuum- or argon-grown crystals. Although this difference is most likely due to the presence of hydrogen at dislocations, the detailed mechanism by which the hydrogen changes the scattering cross-section is not known at this time. The fact that the effect persists long after the decay of free carriers, as evidenced by the decay of the electron cyclotron resonance signal, suggests that some of the electrons may get trapped by dislocations and still retain some mobility along the dislocation lines (*23*). It is these mobile

electrons which may be giving rise to the four-line spectrum, although the possibility that a different scattering center is responsible has not been ruled out.

One may argue that not a single piece of evidence presented thus far is very conclusive as to the origin of the lines. When taken *together*, however, they build a convincing argument for the interpretation that the spectra are the electrically detected magnetic resonance of electrons at dislocations. The next step is to try to deduce from the results something about the microscopic structure of the dislocations.

Distortion of the Dislocation Dangling Bonds.

Returning to expression [5] for the symmetry axes of the dislocation dangling bond spectrum, the quantity α is a measure of the deviation of the axes away from a $\langle 111 \rangle$ direction. Figure 15 shows the six possible tilt directions associated with the $\langle 111 \rangle$ axis. Since the anisotropy of the g-tensor results from the anisotropy of the orbital contribution to g, the g-tensor symmetry axis coincides with the dislocation dangling bond axis. Let δ be the angle between the dislocation dangling bond and the $\langle 111 \rangle$ direction. Then

$$\cos \delta = \frac{\langle 111 \rangle}{\sqrt{3}} \cdot \left[\frac{\langle 111 \rangle}{\sqrt{3}} + 0.021 \frac{\langle 1\bar{1}0 \rangle}{\sqrt{2}} \right] (1 + 0.021^2)^{-\frac{1}{2}} \qquad [7]$$

or $\delta = 1.2°$.

The 1.2° tilt of the dislocation dangling bonds may be an intrinsic distortion characteristic of the dislocation or it may be the result of a Peierls-like instability. There are several distortion geometries, shown in Figure 16, consistent with the data: (a) All dangling bonds in

one dislocation are tilted in the same direction, and along the dislocation line. (b) The dangling bonds are tilted alternately in opposite directions along the dislocation line. (c) The dislocation dangling bonds are tilted in the direction of the Burgers vector. In principle, one could test for possibility (c) by selectively inducing dislocations in one direction and then observing the tilt direction in the EPR g-tensor axis.

The distortion shown in Figure 16(b) is what one would expect if the system had undergone a Peierls-like transition. Peierls (*24*) showed that a uniformly spaced linear chain of atoms with one electron per site undergoes a spontaneous dimerization. A completely analogous instability occurs in a uniformly spaced linear chain of spins coupled by nearest neighbor antiferromagnetic exchange. In this spin-Peierls transition the uniform antiferromagnet is unstable with respect to spin lattice dimerization into an alternating antiferromagnet (*25*). It is unclear at this time which, if any, of these Peierls transitions is taking place along the dislocations in Ge. Grazhulis, Kveder, and Osipyan (*26*) observed a dramatic drop in the magnetic susceptibility of the dislocation spin system in silicon at T = 50 K. They interpreted this drop as being due to an instability with respect to the pairing of neighboring dangling bonds to form singlet pairs (S = 0). Unfortunately, the use of the Ge sample as a high Q cavity precludes such a temperature dependence study in this case.

Conclusions.

The results presented here were all obtained using as-grown crystals and consequently reflect the properties of dislocations formed during crystal growth, as opposed to those created via plastic deformation. The detection of such low dislocation densities was only possible through the use of the ultrasensitive techniques of high Q self-resonant samples and electric detection of magnetic resonance.

No paramagnetism was observed in the ground state (i.e., in the absence of optical excitation). There are two equally acceptable explanations for this. The first is that the spins are all paired, leaving an $S = 0$ configuration. The second is that the spins are so few in number that they can only be electrically detected, this requiring the prior introduction of current carriers.

Paramagnetic centers were observed in optically excited crystals. Some of these centers had the symmetry of the dislocation dangling bonds, with a six-fold 1.2° distortion. The others had the symmetry of the ⟨111⟩ crystal axes, and may be the photo-excited electrons conducting along dislocations. The sign reversal and excitation-decay properties of the lines support the conclusion that free carriers become trapped in a long-lived dislocation conduction band with spin-dependent mobility. There was no evidence of the superparamagnetism (strings of spins coupled to form $S > 1/2$ species) reported by Schmidt, Weber, Alexander, and Sander (*27*) for dislocated Si.

Finally, this same technique has been extended to study the interaction of impurities with dislocations. Specifically, lithium diffused

into a germanium crystal results in an entirely new dislocation spectrum (*28*), presumably due to a lithium ion-dislocation dangling bond complex.

I would like to thank J. W. Bray, E. E. Haller, A. M. Portis, L. M. Falicov, and C. D. Jeffries for many useful comments on this work. I am also grateful to W. L. Hansen and E. E. Haller for providing the Ge crystals. This work was supported by the Director, Office of Energy Research, Office of Basic Energy Sciences, Materials Science Division of the U.S. Department of Energy under Contract Number DE-AC03-76SF00098.

References

(1) Readers unfamiliar with this technique are referred to Charles P. Poole, Jr., "Electron Spin Resonance" (Interscience Publishers, 1967) and to A. Abragam and B. Bleaney, "Electron Paramagnetic Resonance of Transition Ions" (Clarendon Press, Oxford, 1970).

(2) James W. Corbett, Richard L. Kleinhenz, and Neal D. Wilsey, "Electron Paramagnetic Resonance in Semiconductors" in Materials Research Society Symposia Proceedings Volume 2, Defects in Semiconductors (North-Holland, 1981).

(3) D. K. Wilson, Phys. Rev. 134, A265-A286 (1964).

(4) "Dislocations in Solids", Volume 5, edited by F. R. N. Nabarro (North-Holland, 1980).

(5) See, for example, Journal de Physique, Colloque No. 6, Supplement C-6 (1979).

(6) J. Hornstra, J. Phys. Chem. Solids 5, 129 (1958).

(7) H. Alexander, R. Labusch, and W. Sander, Solid State Commun. 3, 357 (1965) (in German).

(8) B. C. Cavenett, Advances in Physics 30, 475 (1981).

(9) A. Honig, Phys. Rev. Lett. 17, 186 (1966).

(10) D. J. Lepine and J. J. Prejean, Proceedings of the 10th International Conference on the Physics of Semiconductors, Cambridge, Mass. (1970).

(11) V. V. Kurylev and S. N. Karyagin, Phys. Stat. Sol. (a) 21, K127 (1974).

(12) S. N. Karyagin, Phys. Stat. Sol. (a) 68, K113 (1981).

(13) V. A. Grazhulis, V. V. Kveder, Yu. A. Osip'yan, JETP Lett. 21, 335 (1975).

(14) T. Wosinski and T. Figielski, Phys. Stat. Sol. (b) 71, K73 (1975).

(15) T. Wosinski, T. Figielski, and A. Makosa, Phys. Stat. Sol. (a) 37, K57 (1976).

(16) W. Szkielko, Phys. Stat. Sol. (b) 90, K81 (1978).

(17) A. Okaya and L. F. Barash, Proc. IRE 50, 2081 (1962), and E. E. Haller and L. M. Falicov, Phys. Rev. Lett. 41, 1192 (1978).

(18) E. J. Pakulis and C. D. Jeffries, Phys. Rev. Lett. 47, 1859 (1981).

(19) R. E. Pontinen and T. M. Sanders, Jr., Phys. Rev. 152, 850 (1966).

(20) E. E. Haller and L. M. Falicov, Phys. Rev. Lett. 41, 1192 (1978).

(21) Laura M. Roth, Phys. Rev. 118, 1534 (1960).

(22) E. Weber and H. Alexander, J. Phys. (Paris), Colloq. 40, C6-101 (1979).

(23) For evidence of quasi one-dimensional conduction along dislocations in other materials see, for example, C. Elbaum, Phys. Rev. Lett. 32, 376 (1974) and V. A. Grazhulis, V. V. Kveder, V. Yu. Mukhina, and Yu. A. Osip'yan, JETP Lett. 24, 142 (1976).

(24) R. E. Peierls, Quantum Theory of Solids, Lecture Notes (1953).

(25) I. S. Jacobs *et al.*, Phys. Rev. B 14, 3036 (1976).

(26) V. A. Grazhulis, V. V. Kveder, and Yu. A. Osip'yan, Phys. Stat. Sol. (b) 103, 519 (1981).

(27) U. Schmidt, E. Weber, H. Alexander, and W. Sander, Solid State Commun. 14, 735 (1974).

(28) E. J. Pakulis, Ph.D. Thesis, University of California, Berkeley, CA (1982).

Table 1. List of Filters

Germanium filter - 2 mm thick

Neutral density filters - 3, 10, 20, 30 db

Long wavelength pass filters -

	5% Wavelength	50% Wavelength	Transmission	Material	Size	Thickness
A	3.4600	3.5400	90%	Ge	1" D	0.040"
B	2.9000	2.9495	63%	Ge	1" D	0.037"
C	2.4340	2.5087	80%	Sapphire	1" D	0.060"
D	2.0500	2.1100	80%	Glass	1" D	0.040"

Wavelengths in microns.

Transmission at maximum.

Long pass filters purchased from Valtec Corporation.

Table 2. Sample Characteristics

Boule Number	Axis	Growth Atmosphere	Crucible	Dimensions, Shape	Orientation	N_D-N_A (cm^{-3})	Etchpits (cm^{-2})	Donor
S-17	⟨100⟩	H_2	Quartz	12.5mm D C	⟨100⟩	$8x10^{13}$	$2x10^4$	As
				8x10x10mm R	⟨100⟩			
				6x8x10mm R	⟨110⟩			
S-29	⟨100⟩	H_2	Quartz	12.5mm D C	⟨110⟩	$7x10^{12}$	0	As
S-61	⟨100⟩	H_2	Quartz	12.5mm D C	⟨110⟩	$2x10^{12}$	$2x10^3$	As
S-62	⟨100⟩	H_2	Quartz	12.5mm D C	⟨110⟩	$1x10^{12}$	$2x10^3$	As
464	⟨100⟩	H_2	Quartz	12.5mm D C	⟨100⟩	$3x10^{12}$	$6x10^3$	P, As
574	⟨100⟩	H_2, D_2 1:1	Quartz	12.5mm D C	⟨110⟩	$5x10^9$	$5x10^4$	?
518	⟨100⟩	D_2	Quartz	12.5mm D C	⟨110⟩	$1x10^{12}$	$1x10^4$	P
139	⟨100⟩	Vacuum	Quartz	12.5mm D C	⟨110⟩	$2x10^{12}$	$1x10^4$	P
400	⟨111⟩	Argon	Graphite	4x10x11mm R	⟨110⟩	$4x10^{12}$	$5x10^3$	P

C: Right circular cylinder; R: Rectangular parallelepiped; D: Diameter.

Table 3. Spectroscopic Splitting Factor in Ge

Center	$g_\perp$	$g_\parallel$	g^i	g⟨100⟩	Reference
4-line spectrum	1.94	0.34		1.59	This work
24-line spectrum	1.89	0.73		1.60	This work
Substitutional P	1.93^s	0.83^s	1.563	1.647	3
Substitutional As	1.92^s	0.87^s	1.570	1.647	3
Substitutional Sb				1.561	19
Substitutional Bi			1.567		3
Surface Sb	1.917	0.83		1.636	19
LiO Complex	1.91	0.85		1.63	20
Intrinsic Surface State 1			2.008		11, 12
Intrinsic Surface State 2			2.003		11, 12
Conduction Electron	2.07^c	0.98^c	1.71^c	1.78^c	21

s: Determined from experiments on stressed crystals.

c: Calculated values.

i: Isotropic value $g^i = 1/3\ g_\parallel + 2/3\ g_\perp$.

Figure Captions

Figure 1. Dislocations of the screw and edge types.

Figure 2. Germanium crystal structure including one 60°-dislocation line, d, with its row of dislocation dangling bonds, and Burgers vector, $\vec{b}$. See reference 6.

Figure 3. Block diagram of the apparatus.

Figure 4. Blowup of the tuneable cavity showing position of sample.

Figure 5. Derivative curves of EPR in As doped Ge (Boule S-17, $N_D-N_A = 8 \times 10^{13}$ cm^{-3}). Magnetic field is oriented along a ⟨100⟩ direction. T = 2°K, f = 25.16 GHz. Note the sign reversal of the new lines as compared to the As hyperfine structure. Dislocation density $\approx 2 \times 10^4$ cm^{-2}.

Figure 6. Angular dependence of the g-tensor for the narrow new lines in a sample of P doped Ge (Boule 518, $N_D-N_A = 10^{12}$ cm^{-3}) as the magnetic field is rotated in a plane tilted ∿3° from a (110) plane. Insert shows the continuation of the lines for low values of g near ⟨110⟩. No data were taken for $g < 1$, corresponding to $H > 19$ kG, the limit of the magnet used. T = 2°K, f = 26.06 GHz, dislocation density $\approx 10^4$ cm^{-2}. The dashed line shows a portion of one of the four broad lines.

Figure 7. Angular dependence of the g-tensor for the narrow lines in a sample of As doped Ge (Boule S-17, $N_D-N_A = 8 \times 10^{13}$ cm^{-3}) as the magnetic field is rotated in a plane tilted ∿3° from a (100) plane. Insert shows the continuation of the lines for low values of g near ⟨110⟩. T ≃ 2°K, f = 24.37 GHz, dislocation density $\simeq 2 \times 10^4$ cm^{-2}. The dashed lines show parts of two of the four broad lines.

Figure 8. Angular dependence of the g-tensor for the four broad lines in a sample of As doped Ge (Boule S-17, $N_D - N_A = 8 \times 10^{13}$ cm^{-3}) as the magnetic field is rotated in the (100) plane. T = 2°K, f = 24.36 GHz, dislocation density $\approx 2 \times 10^4$ cm^{-2}.

Figure 9. Dependence of line shape on excitation intensity, (a) ten times the intensity of (b).

Figure 10. Comparison of the amplitudes of the arsenic hyperfine structure (——o——) and the dislocation lines (——x——) as long pass filters of successively higher energies are used. Filters are indicated along the energy axis at their 50% wavelength energy.

Figure 11. Effect of microwave power in the cavity on the broad lines. (a) 5×10^{-9} watts. (b) 5×10^{-7} watts.

Figure 12. Effect of microwave power in the cavity on the narrow lines. (a) 5×19^{-9} watts. (b) 5×10^{-8} watts.

Figure 13. Amplitude vs. time after closing optical shield. (x) boule 139. (·) boule S-17. (o) arsenic hyperfine structure for comparison.

Figure 14. Spin dependent scattering of photo-excited electrons (bold arrows) by dangling bonds along a dislocation line.

Figure 15. Projection of the Ge crystal structure onto the (111) plane. The heavy labelled lines are the ⟨110⟩ axes in that plane. The six arrows, not to scale, are projections of six of the symmetry directions of the g-tensor for the narrow new lines.

Figure 16. Several possibilities for the projection of the dislocation dangling bonds onto the (111) plane. The dashed lines are dislocations.

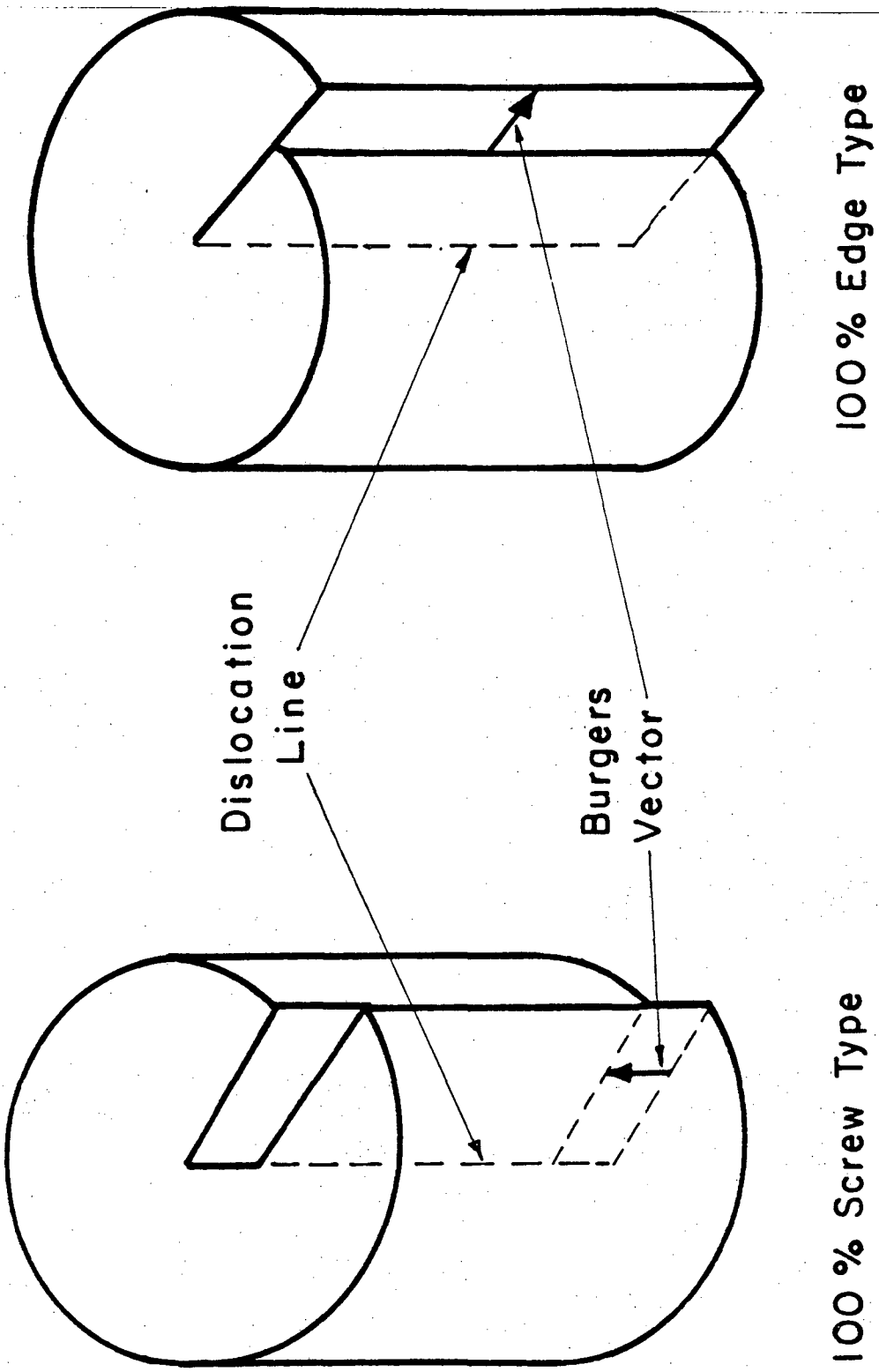

XBL 825-5721

Figure 1

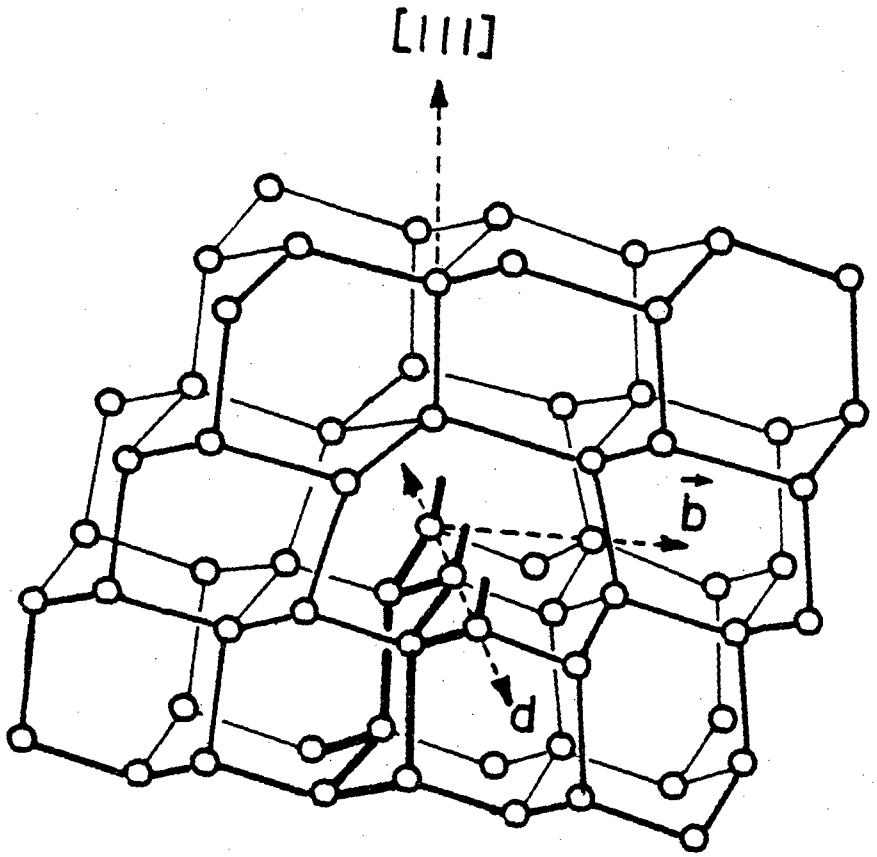

XBL 819-6501

Figure 2

APPARATUS

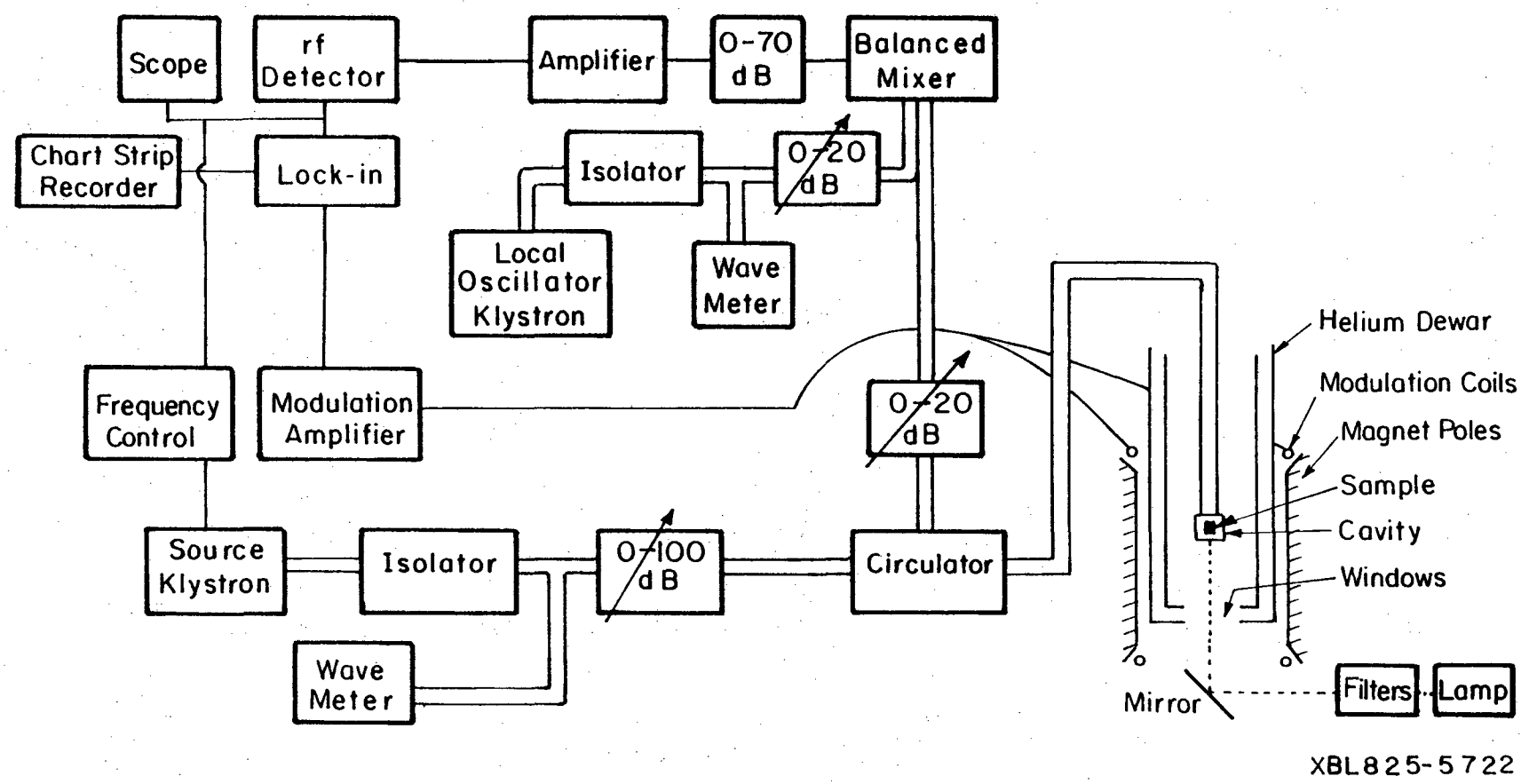

Figure 3

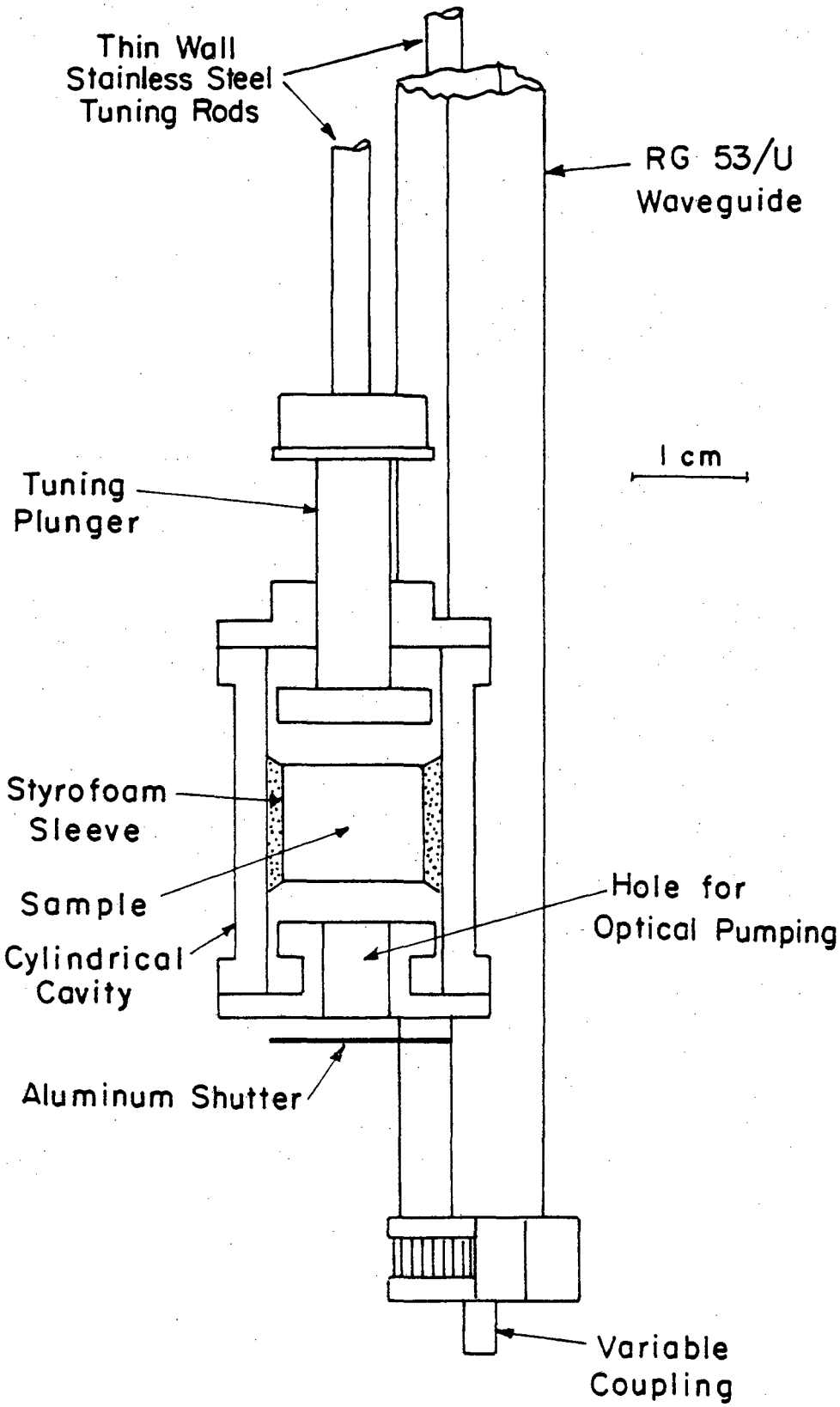

Figure 4 XBL825-5724

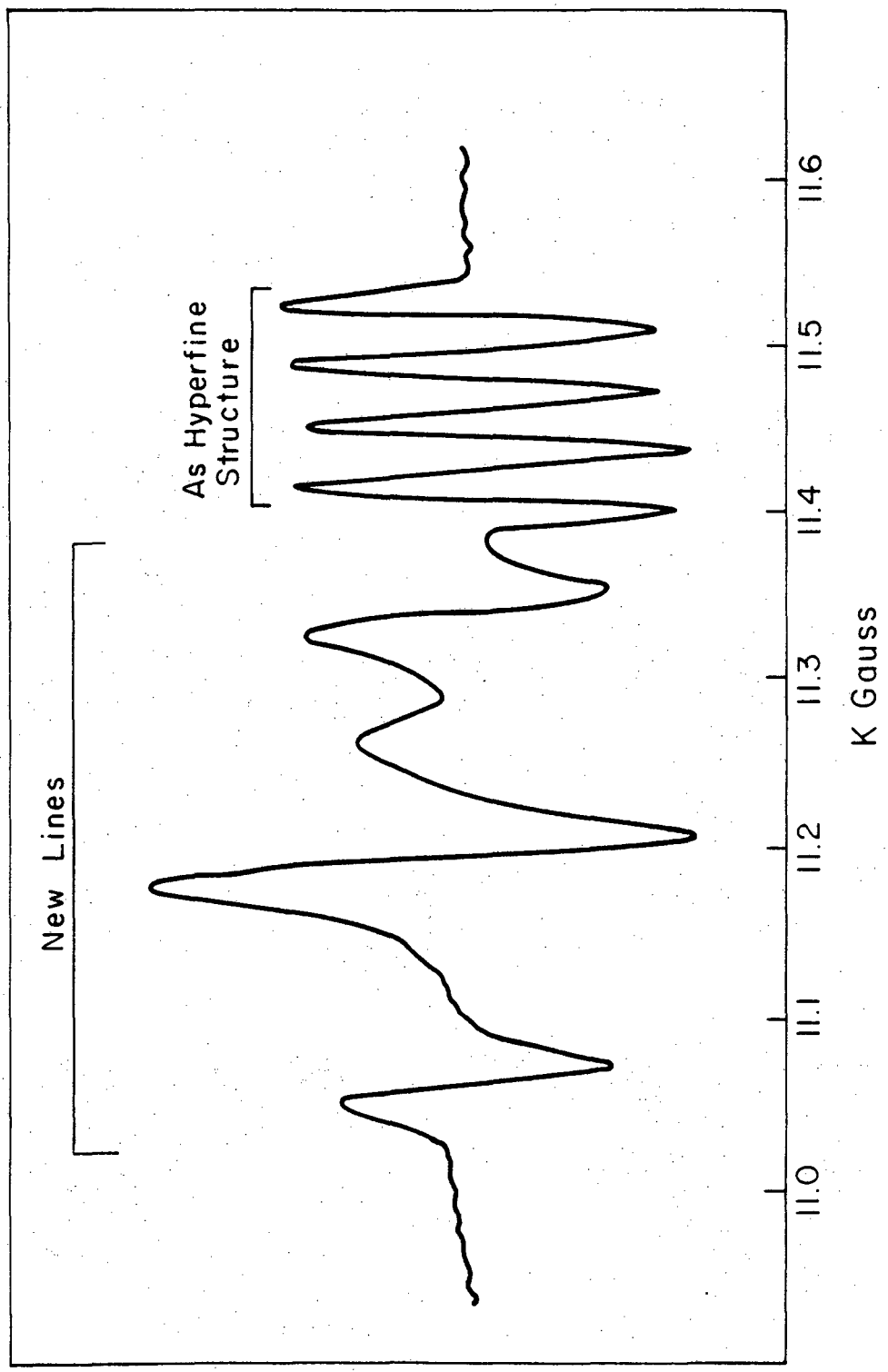

XBL 811-107

Figure 5

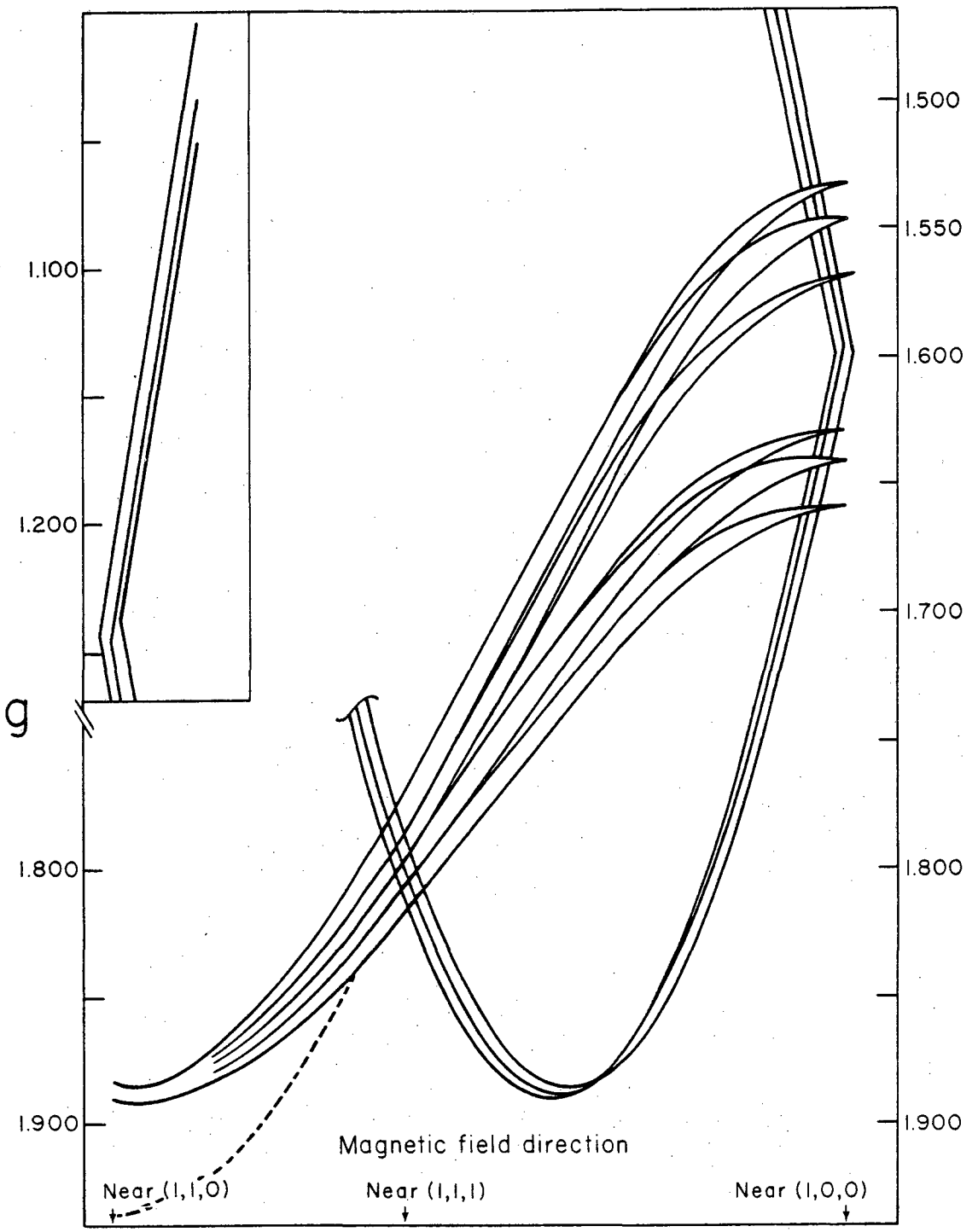

XBL 811-108

Figure 6

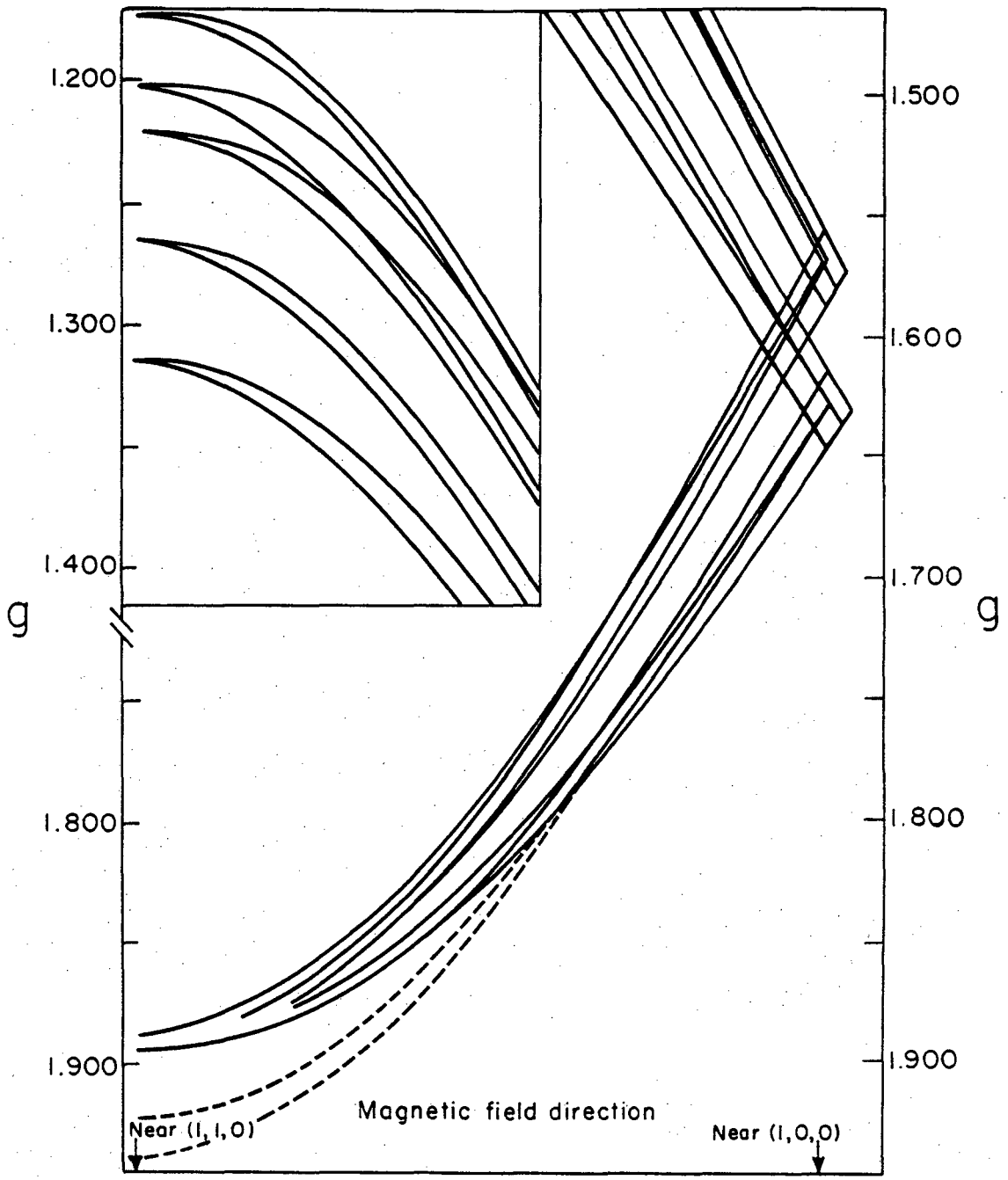

XBL 813-5322

Figure 7

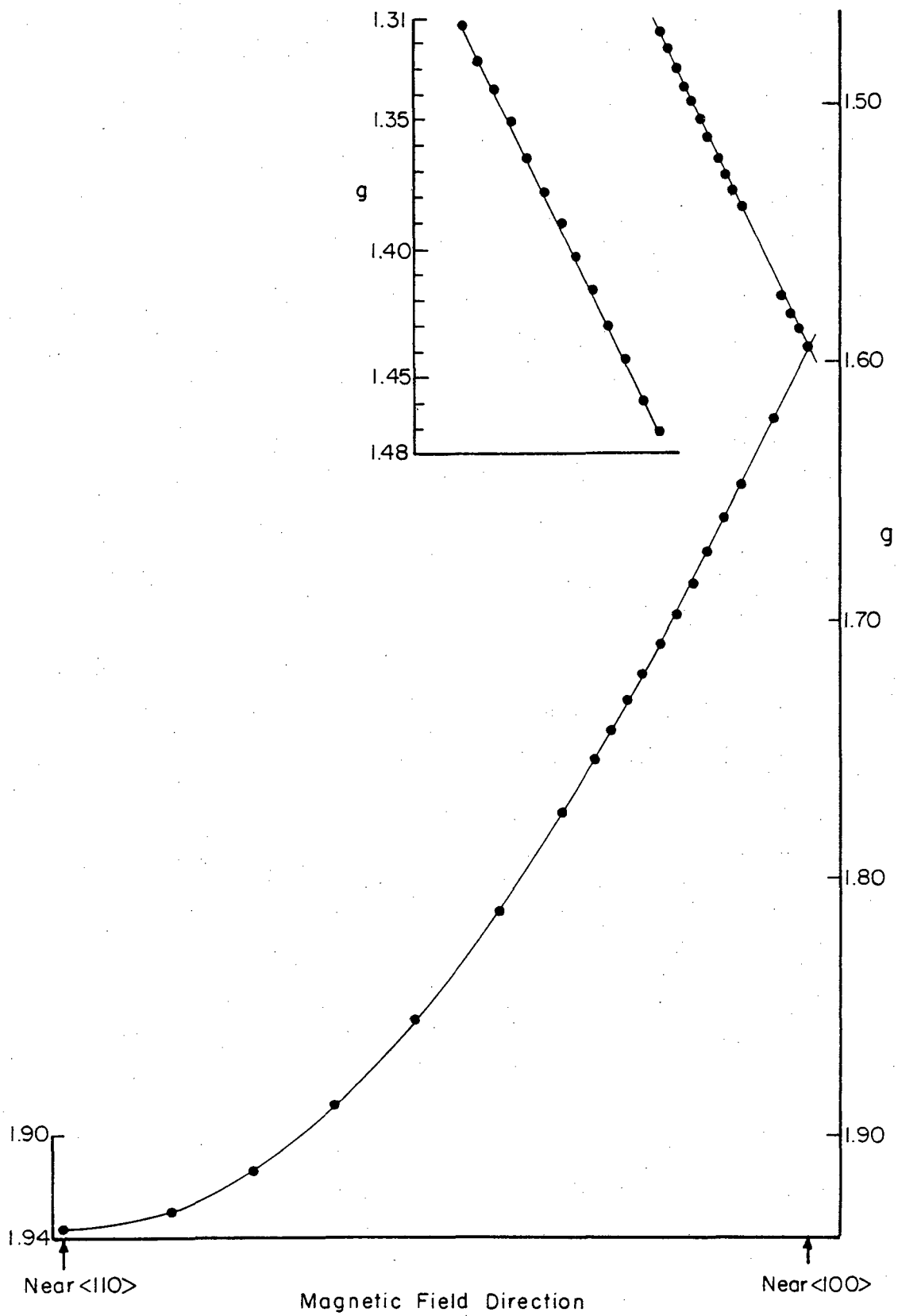

XBL 826-5889

Figure 8

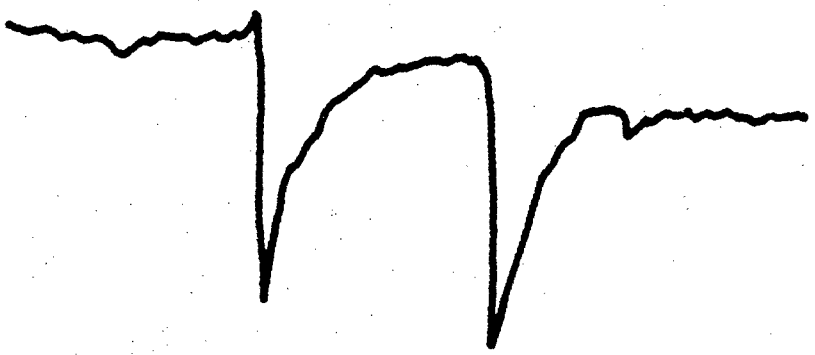

(a)

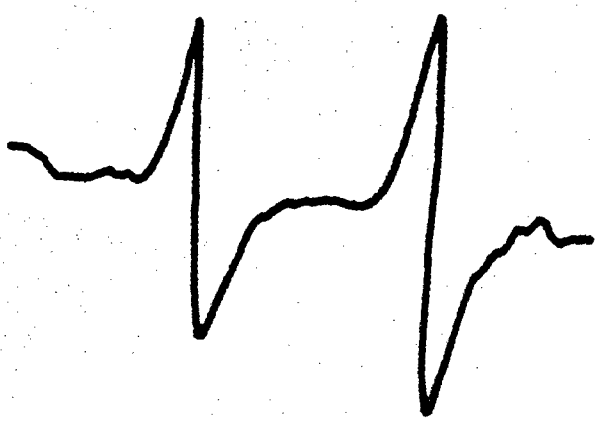

(b)

Figure 9 XBL 826-5882

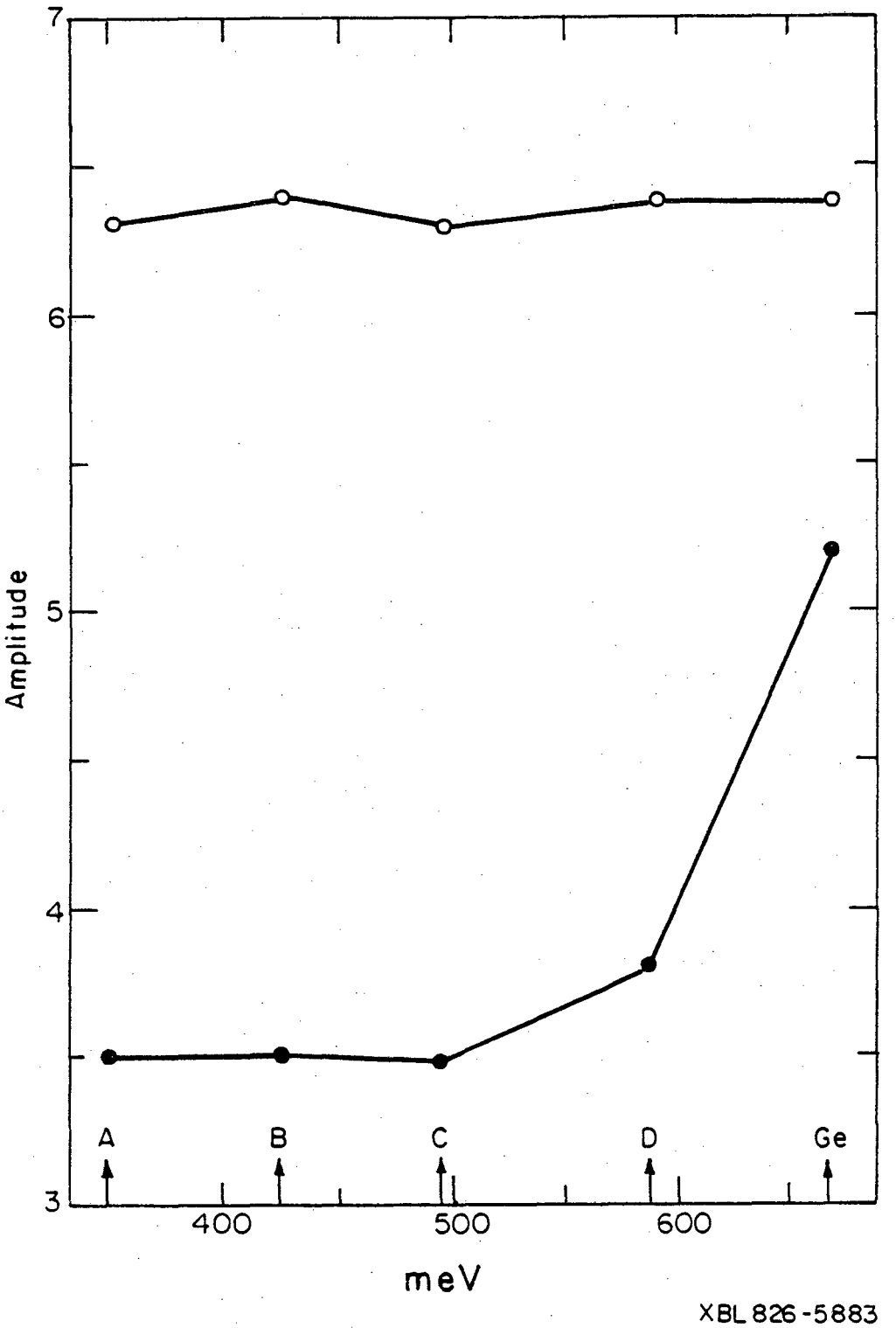

Figure 10

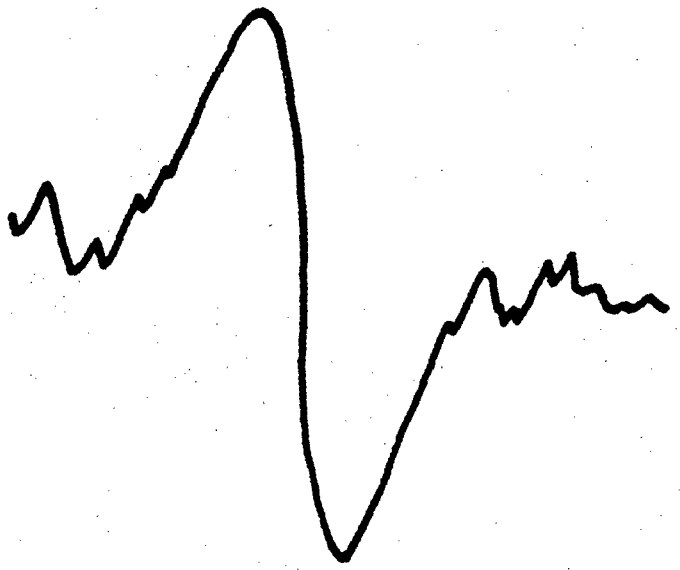

(a)

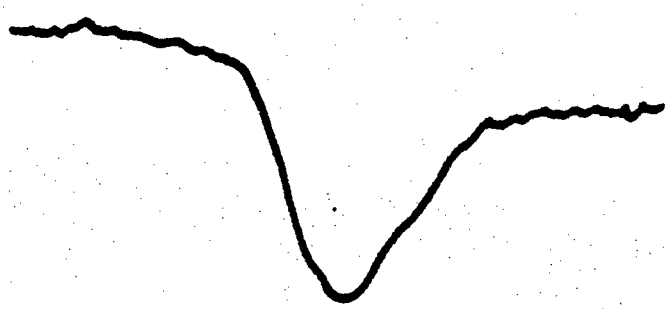

(b)

XBL826-5884 Figure 11

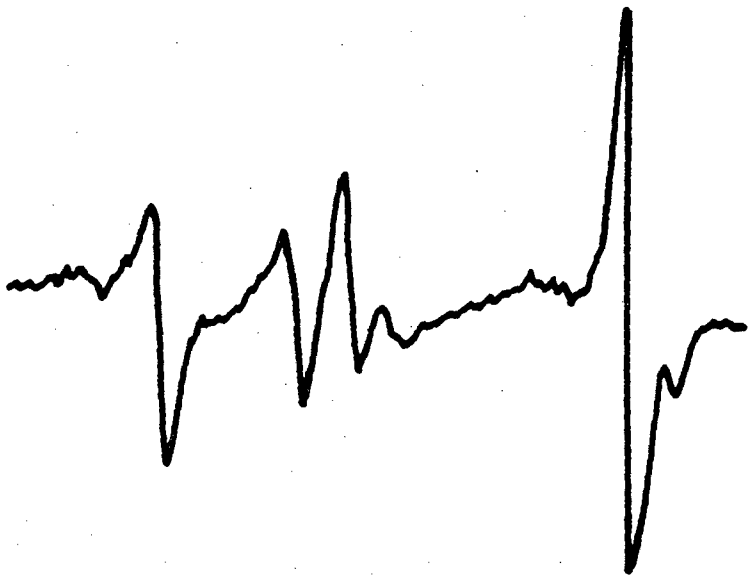

(a)

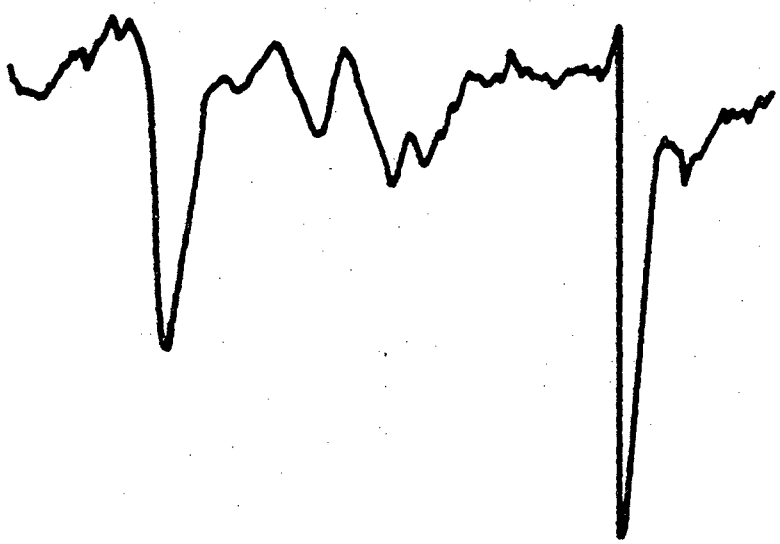

(b)

Figure 12 XBL826-5885

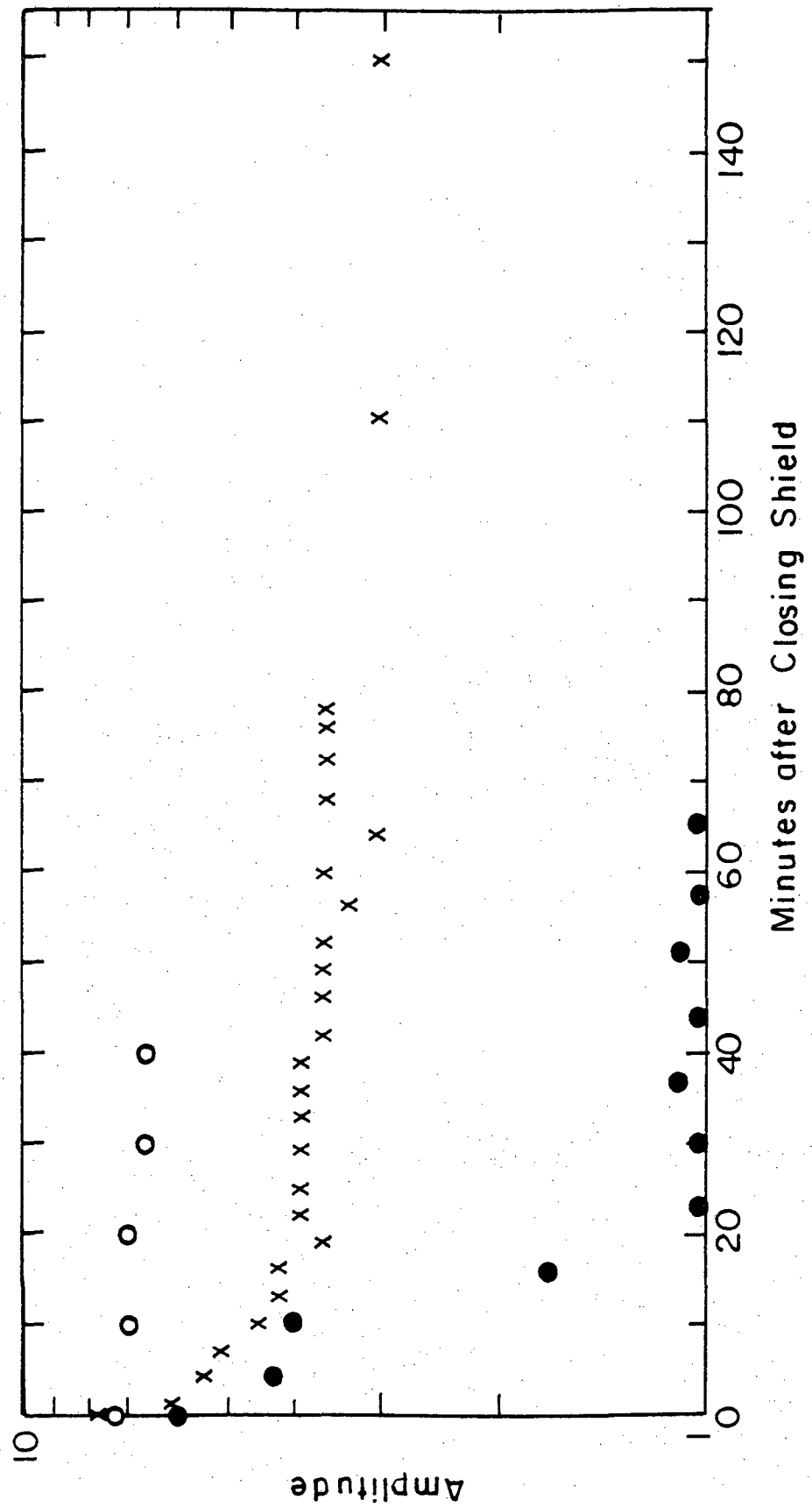

XBL 826-5886

Figure 13

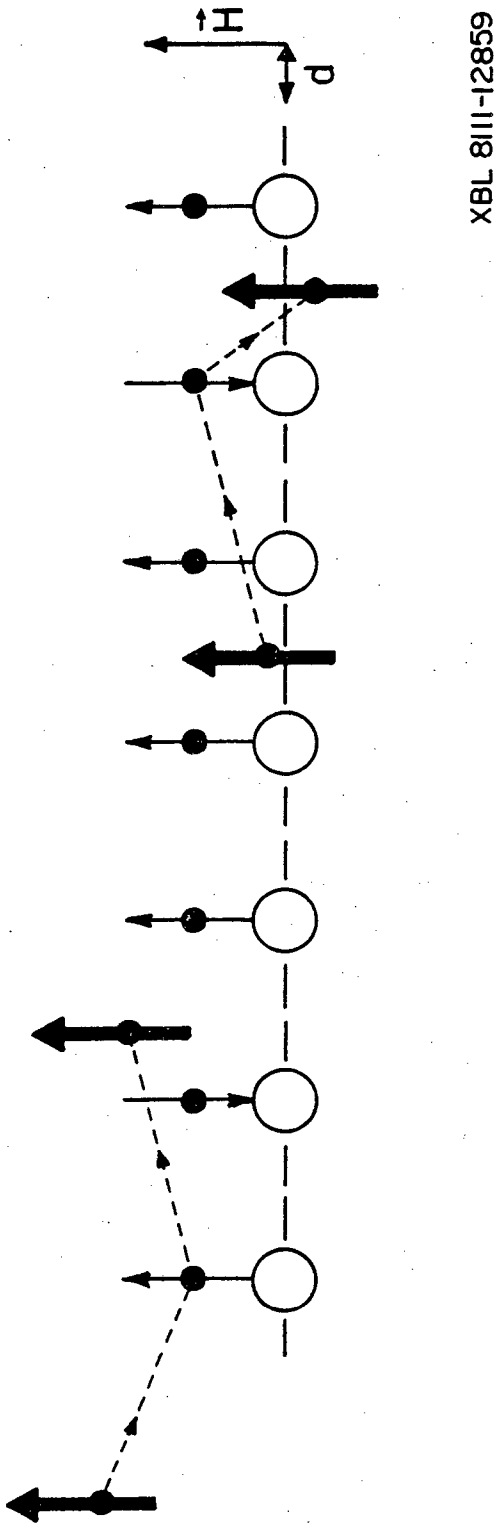

Figure 14

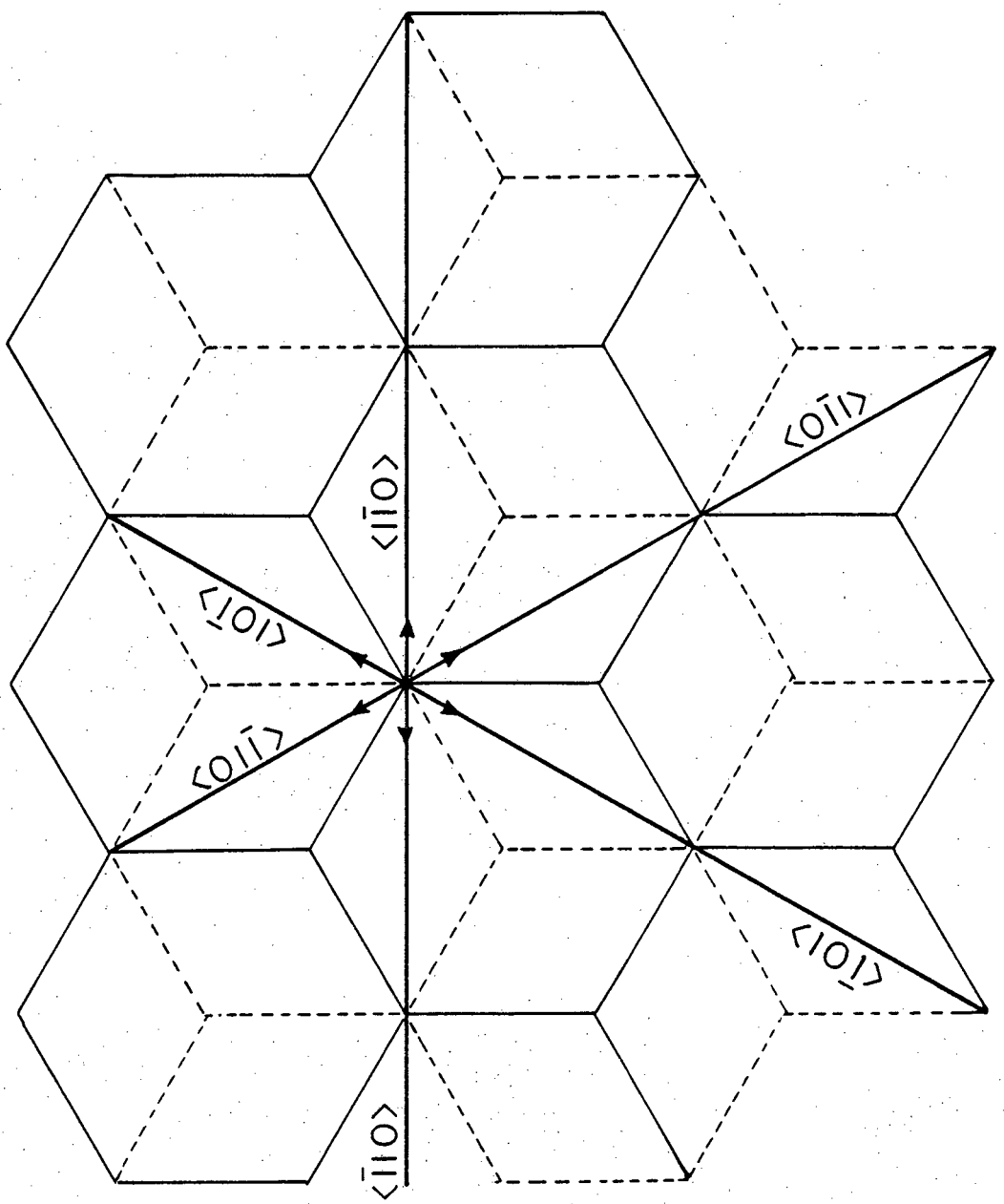

XBL 819-6500

Figure 15

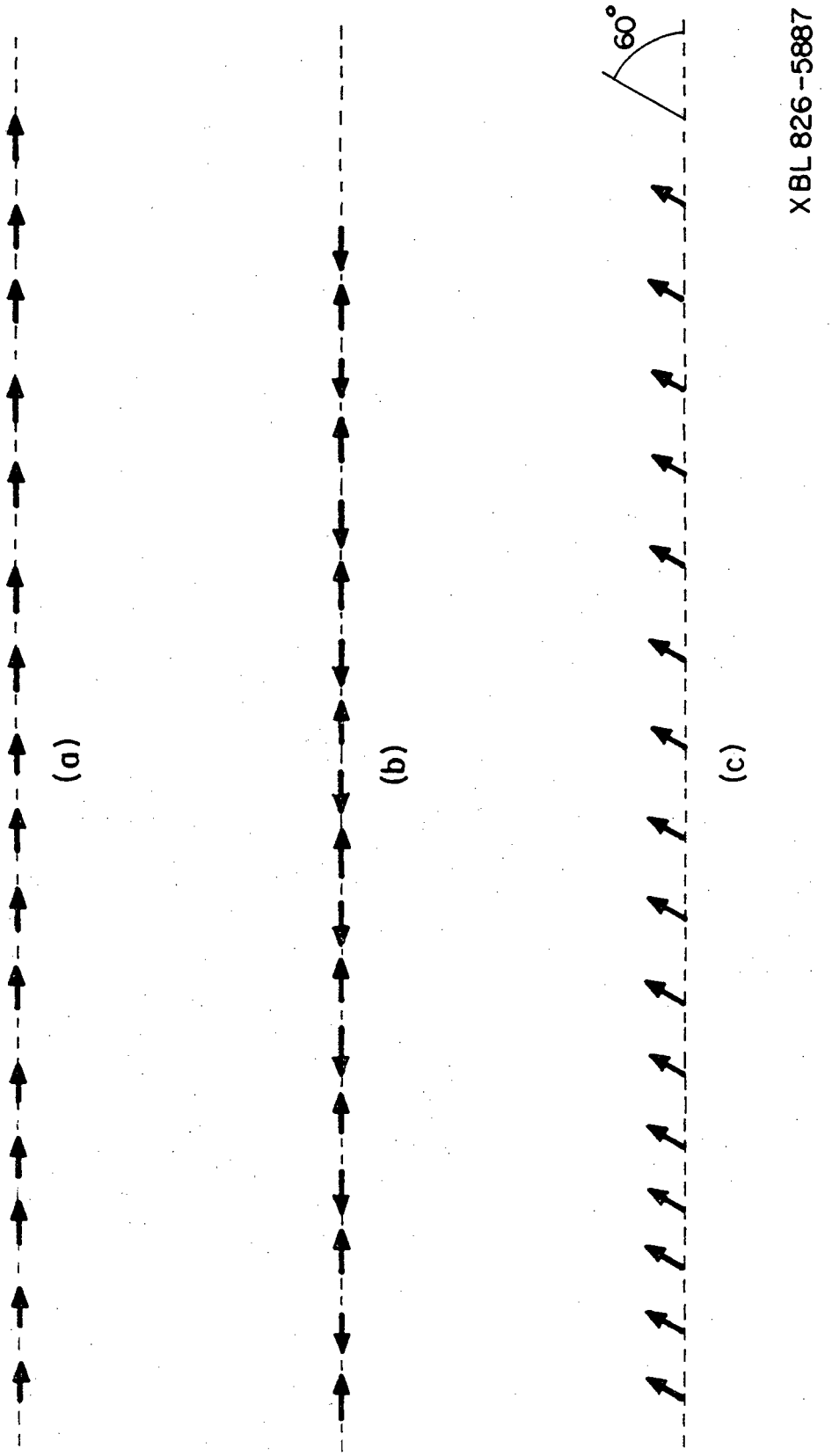

Figure 16

This report was done with support from the Department of Energy. Any conclusions or opinions expressed in this report represent solely those of the author(s) and not necessarily those of The Regents of the University of California, the Lawrence Berkeley Laboratory or the Department of Energy.

Reference to a company or product name does not imply approval or recommendation of the product by the University of California or the U.S. Department of Energy to the exclusion of others that may be suitable.

TECHNICAL INFORMATION DEPARTMENT
LAWRENCE BERKELEY LABORATORY
UNIVERSITY OF CALIFORNIA
BERKELEY, CALIFORNIA 94720